Broadband Time-Domain Measurement System for the Characterization of Nonlinear Microwave Devices With Memory

M. Abouchahine, A. Saleh, G. Neveux, T. Reveyrand, J-P. Teyssier, D. Rousset, D. Barataud, J-M. Nebus

Published in
Microwave Theory and Techniques, IEEE Transactions on
Volume: 58 Issue:4
On pages: 1038 – 1045
April 2010

Digital Object Identifier: 10.1109/TMTT.2010.2042503

Broadband Time-Domain Measurement System for the Characterization of Nonlinear Microwave Devices With Memory

Mouhamad Abouchahine, Alaa Saleh, Guillaume Neveux, Tibault Reveyrand, Jean-Pierre Teyssier, Danielle Rousset, Denis Barataud, and Jean-Michel Nebus

***Abstract*—This paper describes a novel fully calibrated four channel broadband time-domain measurement system for the characterization of nonlinear microwave devices with memory. The hardware architecture of the proposed time-domain measurement system is based on a wideband sub-sampling principle. The sampling heads work at a high strobe signal repetition frequency that can be tuned between 357–536 MHz. We achieve a 40-GHz RF frequency bandwidth and a 160-MHz IF bandwidth. This instrument enables the measurement of carrier and envelope waveforms at both ports of nonlinear microwave devices driven by broadband modulated multicarriers. The test-bench is applied to the cross modulation characterization of a 15-W GaN HEMT CREE *S*-band power amplifier with memory due to different biasing circuit configurations. The amplifier under test is driven by the sum of a large-signal modulated carrier (double-sideband amplitude modulation at 3.6 GHz) and a small single-tone signal at a 110-MHz offset frequency. Our significant contribution comes from the capability of the measurement system to record the time-domain waveforms of several nonadjacent modulated signals on a similar time equivalent scale for different cases of memory effects of the power amplifier under test.**

***Index Terms*—Broadband sub-sampling, GaN power amplifiers, memory effects, nonlinear microwave circuits, time-domain measurements.**

I. Introduction

WIDEBAND communication systems are increasingly used to target multistandard multiband applications. In these communication systems, various architecture design solutions, as well as different modulation standards and multiple access techniques can be implemented, as seen in [1] and [2].

In that context, the characterization of nonlinear devices such as power amplifiers driven by multiple nonadjacent signals is of interest.

Manuscript received June 18, 2009; revised December 20, 2009. First published March 11, 2010; current version published April 14, 2010. This work was performed in the context of the ELOPSYS cluster's Lipsys Project supported by the "Ministère de l'économie des finances et de l'emploi Direction Générale des Entreprises" under Contract 06.2.93.0716.

The authors are with the XLIM Laboratory, UMR 6172, University of Limoges, 87060 Limoges Cedex, France (e-mail: mouhamad.abouchahine@xlim.fr; alaa.saleh@xlim.fr; guillaume.neveux@xlim.fr; tibault.reveyrand@xlim.fr; jean-pierre.teyssier@xlim.fr; danielle.rousset@xlim.fr; denis.barataud@xlim.fr; jean-michel.nebus@unilim.fr).

Color versions of one or more of the figures in this paper are available online at http://ieeexplore.ieee.org.

Digital Object Identifier 10.1109/TMTT.2010.2042503

The work proposed in this paper focuses on wideband time-domain measurement technique and setup based on the broadband harmonic sub-sampling principle.

Recently, different time-domain measurement systems have been proposed to target the wideband characterization of nonlinear microwave devices. The need for a good tradeoff between dynamic range and frequency bandwidth has led to the use of microwave transition analyzers [3], digital storage oscilloscopes [4], [5], or large-signal network analyzers [6], [7].

Large-signal network-analyzer measurements based on the harmonic sub-sampling principle performed at 20 MHz have demonstrated great interest for nonlinear microwave device characterization. Nevertheless, significant complexity arises when measurements of signals having envelope bandwidths wider than 10 MHz are required. This is due to low-frequency repetition rate of the strobe signal. Time-domain measurements of wideband multisines requiring complex processing techniques and specific control of the strobe frequency have been proposed in [7] and [8]. The complexity of these techniques is due to the hardware frequency limitation of sampling heads.

In [9], we proposed a new architecture based on the use of sampling heads working with a high-repetition frequency strobe signal (from 350 to 540 MHz) that enables wideband time-domain measurements. 60-MHz bandwidth have been yet performed and demonstrated in [9].

This paper presents an extended description of the main characteristics of the broadband sampler based instrument, such as gain conversion versus IF and RF frequencies. We report up to 110-MHz envelope bandwidth measurements. We also focus on time-domain envelope waveform measurements applied to the characterization of a power amplifier exhibiting memory effects depending on its biasing circuit configuration. Additional insights are mentioned to prove the capability of the setup to perform simultaneous time-domain envelope waveforms at different carriers.

To conclude, we mention the potential use of the measurement tool for behavioral modeling of wideband nonlinear devices with memory.

II. Description of the Measurement System

A. Hardware Configuration for Wideband Measurements

The proposed instrument is based on the harmonic sub-sampling principle, which enables the downconversion of microwave spectra into IF spectra. The downconvertor is the key component of the instrument.

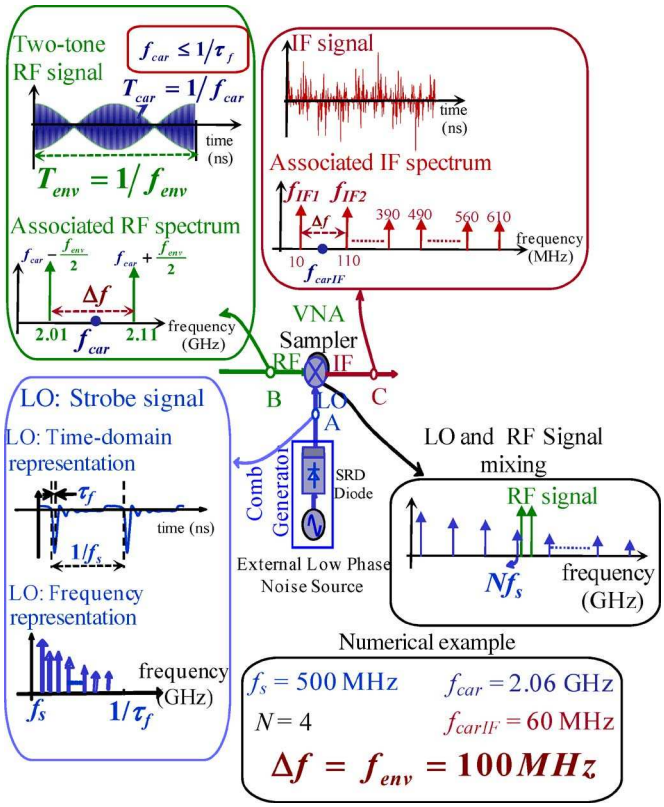

Fig. 1. Numerical example of a broadband sub-sampling principle applied to a two-tone RF signal.

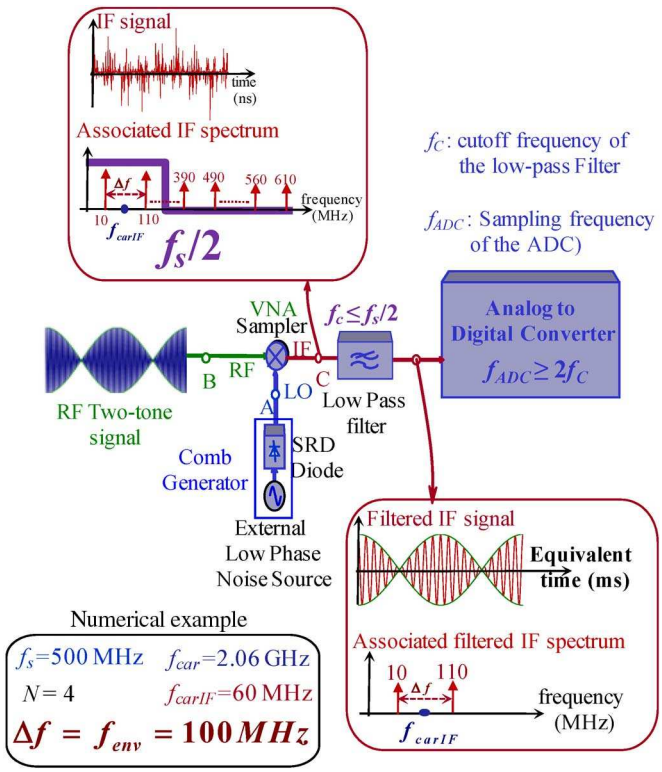

Fig. 2. Simplified block diagram of a channel based on the sub-sampling principle for a large bandwidth two-tone RF signal.

With this instrument, measurements of voltage and current time-domain waveforms are performed at both ports of devices by capturing the whole wave spectra in a single shot. In the following, it is applied to a 50-Ω matched power amplifier. Current and voltage waveform measurements reported in this paper are linked by 50-Ω impedance.

The RF input signal is mixed with a strobe signal, which is a repetitive pulse, as shown in Fig. 1 for a two-tone input RF signal. The envelope period of the two-tone input RF signal, the RF carrier frequency, and the sampling frequency driving the comb generator are, respectively, noted $T_{\rm env}$, $f_{\rm car}$, and f_s, in Fig. 1.

The RF frequency bandwidth is directly linked to the duration of the pulse (τ_f in Fig. 1) and in particular to the falling time of the pulse. The mixing principle results in an output spectrum that requires a filtering of aliasing products, as depicted in Fig. 2, in order to obtain an IF spectrum that is a translated and compressed image of the RF spectrum. It can be observed in Fig. 2 that only the mixing product of the RF signal with the fourth component of the strobe signal ($N = 4$ in Figs. 1 and 2) can be useful to extract an IF image of the broadband two-tone RF signal. The period of the pulse repetition rate determines the cutoff frequencies of the IF filter. This principle requires the knowledge of the RF spectrum frequencies to ensure a unique relationship between the original periodic RF signal and the measured IF signal. The filtered intermediate signal is a two-tone signal (at $f_{\rm IF1}$ and $f_{\rm IF2}$) that corresponds to an amplitude modulation at the frequency $f_{\rm carIF}$ equal to 60 MHz.

The value of the cutoff frequency of the low-pass filter seen in Fig. 2 in commercially available instruments is currently limited to 10 or 20 MHz. Fast analog to digital converters (ADCs) with a high dynamic range are used and are very well suited for continuous wave (CW) measurements. Nevertheless, the sub-sampling principle, when "naturally" applied to measure multitone signals, as in [5] and [8], suffers from a significant drawback due to IF bandwidth limitation. Different techniques can be used to perform measurements of broadband RF signals, but they are not based on the "natural" unscrambled translation/compression of the RF spectrum [8]. Therefore, they are quite difficult to implement.

The benefits of a high-repetition frequency strobe signal are sketched in Fig. 2 in the case of two-tone measurements. Fig. 2 shows a "natural" unscrambled translation and compression process of the RF input spectrum.

In the work presented hereafter, measurements of broadband modulated signals are more easily and straightforwardly performed by the use of such a kind of strobe signal with a high-frequency repetition rate. For that purpose, sampler parts of a VNA have been used and modified to build a new sampling unit configuration, as shown in Fig. 3.

We built a 160-MHz bandwidth IF stage for signal amplification, antialiasing filtering, and for adjusting the signal to the full scale of ADCs. The IF stage includes two (dc–2 GHz) 30-dB gain monolithic amplifiers and two (dc–160 MHz) ceramic low-pass filters, as indicated in Fig. 3. We obtained good matching conditions and ensured electrical stability and an appropriate signal level to feed ADC circuits.

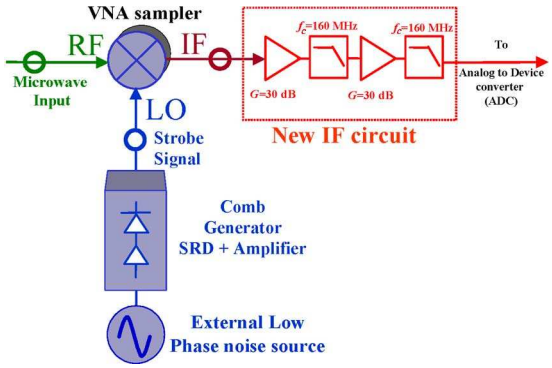

Fig. 3. Modified sampling head for broadband measurements.

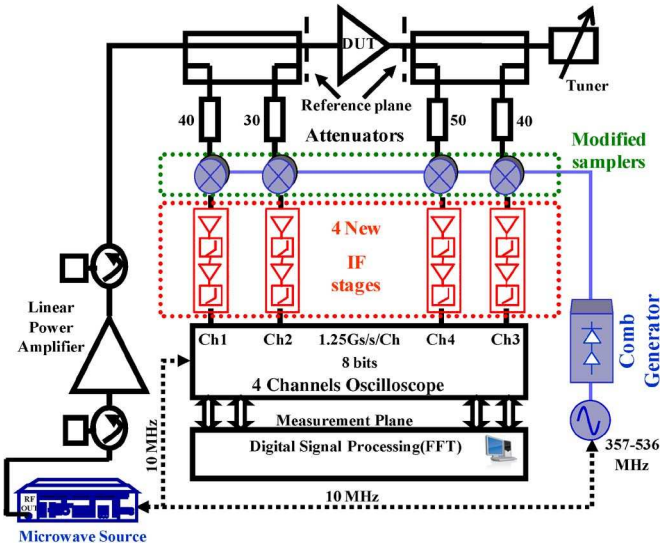

Fig. 4. High-level block diagram of the broadband time-domain measurement setup.

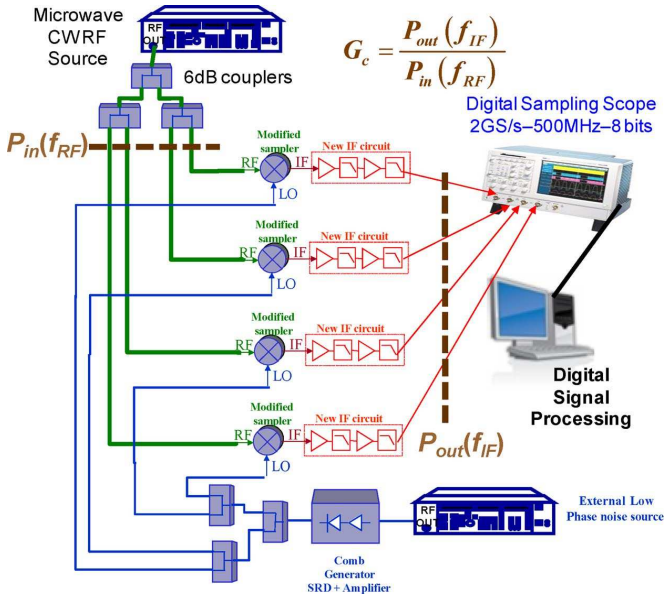

Fig. 5. High-level block diagram of the test bench used to perform gain conversion measurements.

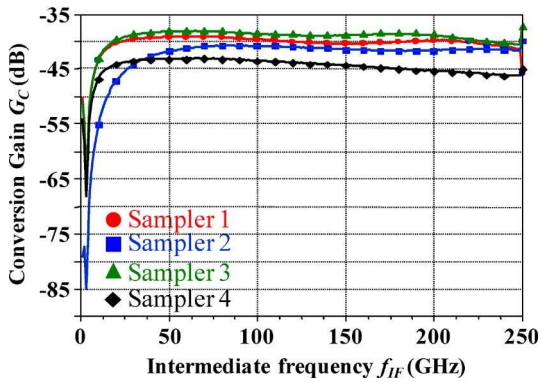

Fig. 6. Conversion gain of the four sampling heads versus the IF frequency.

A low phase-noise source with a tunable frequency in the 357–536-MHz range drives an amplifier and a comb generator based on the use of a step recovery diode. This assembly provides narrow pulses with a high repetition rate and is used to generate the strobe signal of the sampling head.

The modified sampling heads driven by the same low phase-noise source and comb generator have been assembled to build a four-channel measurement instrument. A four-channel 1-Gs/s–8-bit sampling scope has been used for data acquisition. The high-level block diagram described in Fig. 4 is fully computer controlled for data acquisition and signal processing (such as fast Fourier transform (FFT) and error correction matrix computations).

The gain conversion of the four synchronized sub-sampling channels (sampling heads with IF circuits) has been characterized versus the IF output frequency. For that purpose, we used the test bench described in Fig. 5. A microwave CW RF source is used to vary the CW RF signal driving the four modified sampling heads. The magnitude and the frequency of this RF source is variable. The strobe signal can also be adjusted in frequency thanks to an external low phase-noise source and a comb generator.

The gain conversion is defined as the following ratio:

$$G_c = \frac{P_{\text{out}}(f_{\text{IF}})}{P_{\text{in}}(f_{\text{RF}})} \tag{1}$$

The input RF power is measured at the output of 6-dB couplers with a calibrated power meter and the output IF power is measured at the output of the new IF circuit of the modified sampling heads by using a four-channel 1-GS/s–8-bit sampling scope.

Measurement results of the four synchronized sub-sampling channels versus the IF output frequency is shown in Fig. 6. A 250-MHz bandwidth is obtained and is compliant with theory when a 500-MHz strobe signal is applied.

The dynamic range of the built-in measurement system is measured and plotted in Fig. 7. The dynamic range is estimated at 50 dB. The dynamic range could be drastically improved by using 14-bit ADCs instead of our sampling scope.

The measured gain conversion of the four synchronized sub-sampling channels (sampling heads with IF circuits) versus the RF input frequency is shown in Fig. 8.

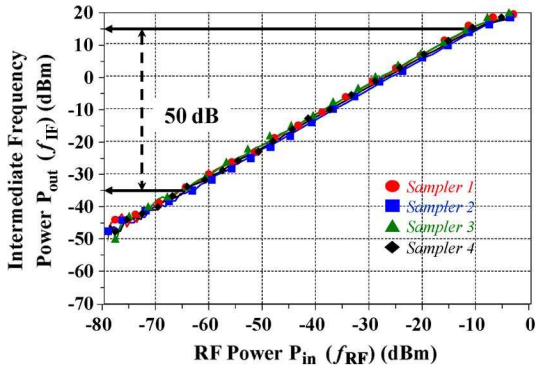

Fig. 7. Measured dynamic range of the four sub-sampling channels.

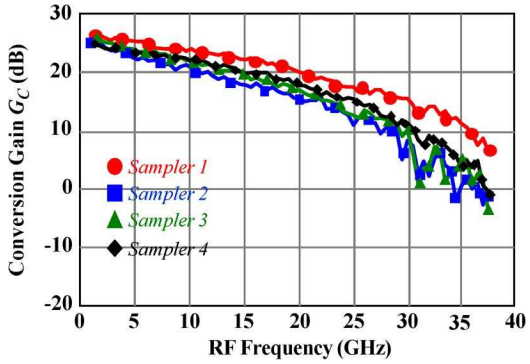

Fig. 8. Measured conversion gain of the four sub-sampling channels (sampling heads with IF circuits).

B. System Calibration Procedure

The purpose of the system calibration procedure is to determine a matrix of error terms linking raw data provided by scope measurement channels with incident and scattered power waves at the device-under-test ports.

The error correction matrix is expressed as follows [2]:

$$\begin{bmatrix} a_1^i \\ b_1^i \\ a_2^i \\ b_2^i \end{bmatrix}_{DST} = K^i \exp(j\varphi^i) \begin{bmatrix} 1 & \beta_1^i & 0 & 0 \\ \gamma_1^i & \delta_1^i & 0 & 0 \\ 0 & 0 & \alpha_2^i & \beta_2^i \\ 0 & 0 & \gamma_2^i & \delta_2^i \end{bmatrix} \begin{bmatrix} a_{1M}^i \\ b_{1M}^i \\ a_{2M}^i \\ b_{2M}^i \end{bmatrix} \quad (2)$$

where i denotes frequency index.

For the first step, a classical short-open-load-thru (SOLT) calibration is made to determine all error terms, except K^i and φ^i. Secondly, a power calibration is done at a relatively high 30-dBm power by using a power sensor and a calibrated 20-dB attenuator. At the end of this step, the K^i coefficients are determined. The relative error coefficients β_1^i, γ_1^i, δ_1^i, α_2^i, β_2^i, γ_2^i, and δ_2^i and the absolute error terms $|K^i|$ are determined by sweeping the frequency of the CW microwave source.

After that, a phase calibration is performed in order to determine the φ^i coefficients. For that purpose, we use a commercially available vector signal generator (VSG), which provides a multisine signal with a maximum bandwidth of 120 MHz. Our standard phase reference signal is built using the calibrated VSG with two subsets of multisine with a 1-MHz tone spacing, and that are spaced 110 MHz away from each other. The shape of this signal spectrum is shown in Fig. 9.

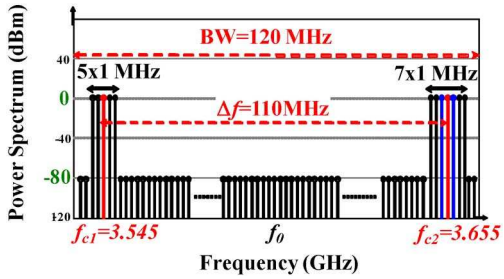

Fig. 9. Spectrum shape of the multisine phase reference signal.

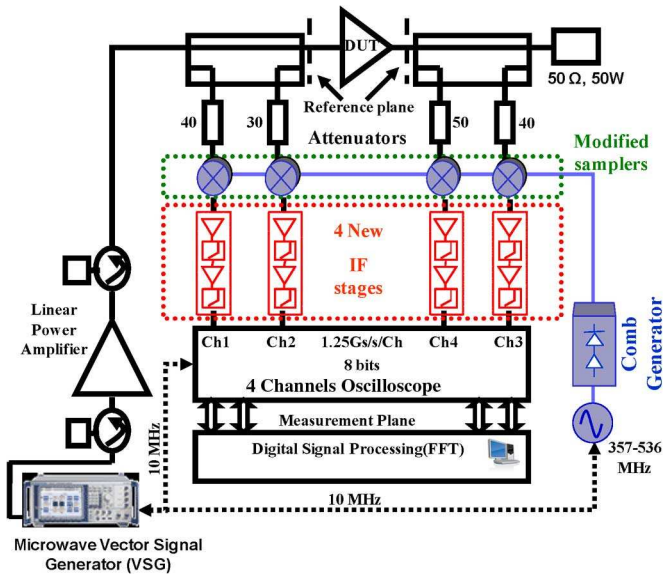

Fig. 10. High-level block diagram of the broadband time-domain measurement setup.

Measurements shown in Section III do not take into account harmonics of carriers, but multiple intermodulation products. Therefore, in this study, we achieved an IF phase calibration so that the group delays of the measurement channels are corrected during the measurements.

III. Measurement Results

In this section, we apply the proposed instrument to the measurements of time-domain waveforms of several nonadjacent modulated signals on a similar time equivalent scale for two different cases of memory effects exhibited by the power amplifier under test. The high-level block diagram of the setup is described in Fig. 10. In this setup, the microwave source is replaced by a 120-MHZ–6-GHz VSG.

We measured a 15-W–16-dB gain S-band 50-Ω matched GaN HEMT CREE power amplifier. The demonstration board of the power amplifier is shown in Fig. 11.

First, the "initial" circuit was characterized. Second, 1- and 33-μF capacitances connected in the drain bias circuit were removed. Although this modification does not impact the quasi-static characteristics of the power amplifier, it may introduce low-frequency memory effects when the device is driven by a large level modulated signal. Large capacitances of the designed bias circuits have been removed for the study in further works

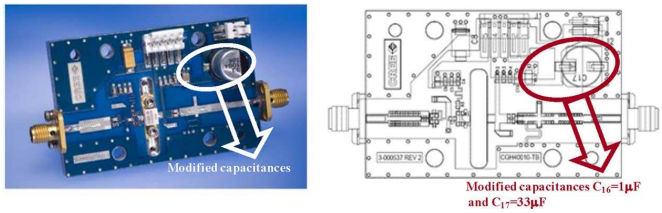

Fig. 11. Demonstration board of the amplifier and bias circuit modification.

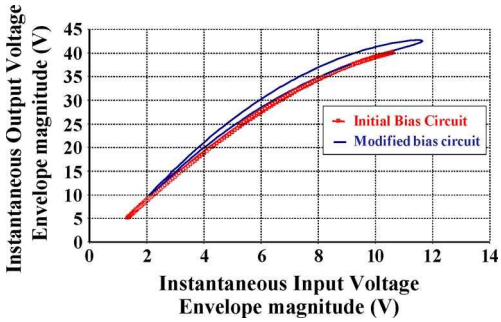

Fig. 12. Dynamic AM/AM characteristics at 31-dBm input average power (compression zone).

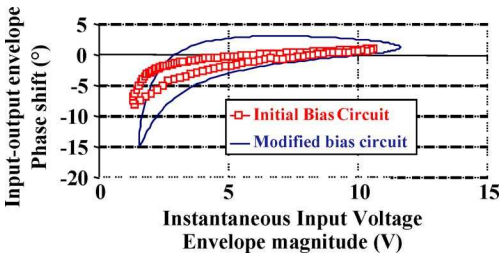

Fig. 13. Dynamic AM/PM characteristics at 31-dBm input average power (compression zone).

of the behavior of amplifiers targeted to be used in envelope tracking techniques [10], [11].

A. Dynamic Power Characteristics of the GaN HEMT CREE Power Amplifier

First, we used the test-bench to extract the dynamic AM/AM and AM/PM characteristics of the 50-Ω matched GaN HEMT CREE power amplifier. Dynamic AM/AM and AM/PM characteristics recorded with a 1-MHz double-sideband amplitude modulation at a 3.655-GHz carrier frequency are given in Figs. 12 and 13. In both cases, the bias conditions are $V_{\mathrm{gs0}} = -2.7$ V, $V_{\mathrm{ds0}} = 28$ V, and $I_{\mathrm{ds0}} = 200$ mA.

Differences observed between AM/AM and AM/PM measurement results prove the presence of low-frequency memory for the modified biasing circuit. This is clearly indicated by the hysteresis shapes observed in Figs. 11 and 12.

The main objective of the work reported here is to demonstrate the capability of the test-bench to characterize the impact of memory effects in the power amplifiers driven by modulated signals.

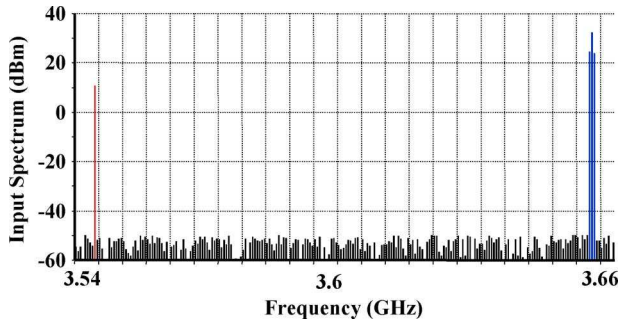

Fig. 14. Corrected input power spectrum for $P_{\mathrm{in}}(f_{c2}) = 31.9$ dBm (compression zone).

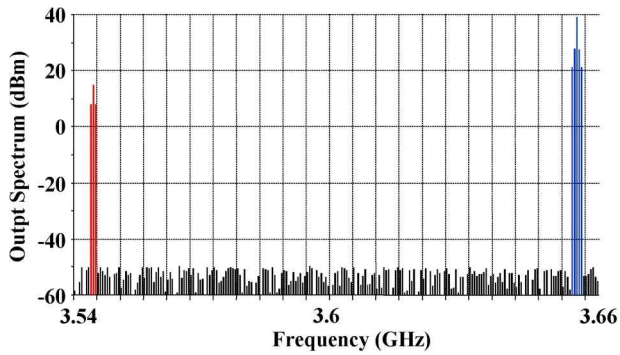

Fig. 15. Corrected output power spectrum for $P_{\mathrm{in}}(f_{c2}) = 31.9$ dBm (compression zone).

B. Time-Domain Waveform Measurements of Several Nonadjacent Modulated Signals

The proposed measurement system is then applied to the time-domain waveform measurements of several nonadjacent modulated signals. The power amplifier with initial and modified drain bias circuit configurations was driven simultaneously by two signals: a large-signal amplitude modulated carrier (31,6% modulation index) at the frequency f_{c2} and a low-level CW nonmodulated carrier at an offset frequency (f_{c1}): $f_{c1} = 3.545$ GHz, $f_{c2} = 3.655$ GHz, and $\Delta f = f_{c2} - f_{c1} = 110$ MHz.

Figs. 14 and 15 represent, respectively, the measured and corrected spectra at the input and output of the amplifier when it is driven in its nonlinear region (compression zone).

Due to the nonlinear behavior of the amplifier, the amplitude modulation at the frequency f_{c2} is transferred to the low-level CW nonmodulated carrier. It can be clearly observed in the frequency domain. It is a challenge to observe such phenomenon in the time domain. The setup presented in Fig. 10 has the capability to extract time-domain waveforms of nonadjacent signals at f_{c1} and f_{c2} on a similar time equivalent scale.

Fig. 16 shows an image of the time equivalent measured output current waveforms of the modulated signal at f_{c2}.

Fig. 17 shows an image of the time equivalent measured output current waveforms of the cross-modulated low-level carrier at $f_{c1} = 3.57$ GHz.

Such time-domain curves recorded at high power driving the amplifier under test provide a visual inspection of the transferred

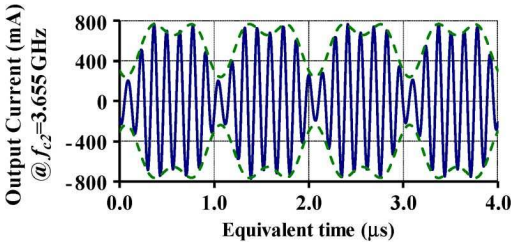

Fig. 16. Time-domain current waveform around f_{c2} at $P_{\text{in}}(f_{c2}) = 31.9$ dBm (compression zone).

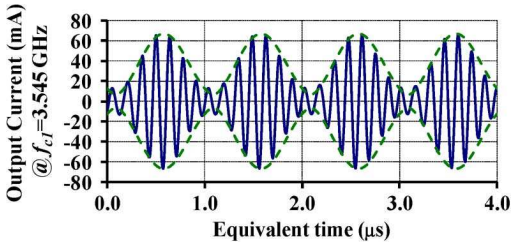

Fig. 17. Time-domain current waveform around f_{c1} at $P_{\text{in}}(f_{c2}) = 31.9$ dBm (compression zone).

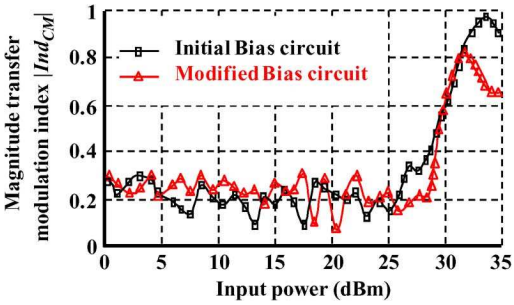

Fig. 18. Magnitude of the modulation index versus average input power.

modulation to the low-level offset frequency. Two specific criteria can be defined to evaluate this transferred modulation: amplitude and phase transfer modulation indices of the low-level offset carrier at f_{c1}

$$|\text{Ind}_{CM}| = \frac{\text{Max}\left(|\text{Env}_{\text{offset\_tone}}|\right) - \text{Min}\left(|\text{Env}_{\text{offset\_tone}}|\right)}{\text{Max}\left(|\text{Env}_{\text{offset\_tone}}|\right) + \text{Min}\left(|\text{Env}_{\text{offset\_tone}}|\right)} \quad (3)$$

$$\angle\text{Ind}_{CM} = \frac{\text{Max}\left(\angle(\text{Env}_{\text{offset\_tone}})\right) - \text{Min}\left(\angle(\text{Env}_{\text{offset\_tone}})\right)}{2} \quad (4)$$

where $|\ |$ denotes the magnitude of the envelope and $\angle$ denotes the phase of the envelope.

Fig. 18 shows the magnitude of the transfer modulation index defined in (3) versus the input power driving the device for the amplifier with the initial and modified bias circuit configurations.

Fig. 19 shows the variations of the phase transfer modulation index defined in (4) versus the input power driving the device for the amplifier with the initial and modified bias circuit configurations.

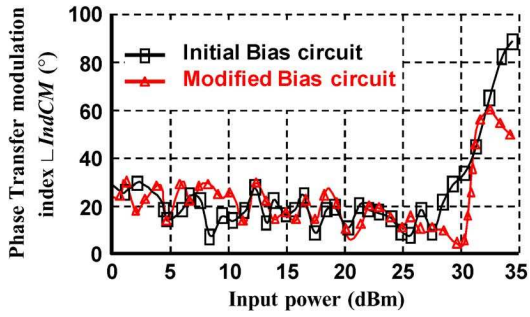

Fig. 19. Phase of the modulation index versus average input power.

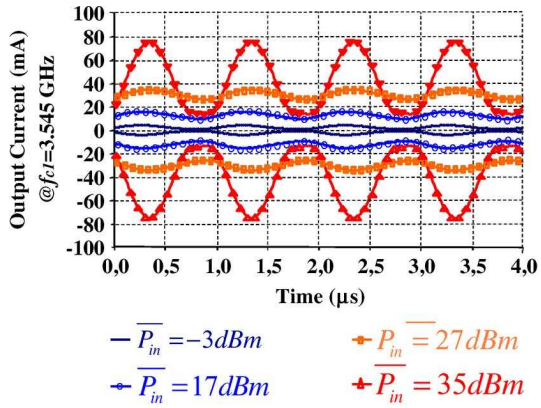

Fig. 20. Output envelope current waveform of the low-level transferred modulated tone at f_{c1} versus the equivalent time and four different average input powers.

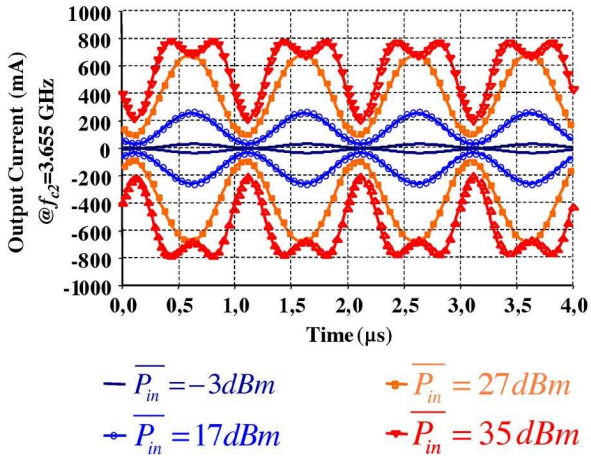

Fig. 21. Output envelope current waveform of the modulated signal at f_{c2} versus the equivalent time and four different average input powers.

Transfer modulation indices remain at zero when the amplifier works in its linear region and a variation appears when the amplifier is driven into its nonlinear operation regime. This variation does not appear for the same input power when the amplifier works with its initial or modified bias circuit configurations.

Fig. 20 shows the measured time-domain envelope waveforms of the large-signal modulated carrier. Fig. 21 presents the measured time-domain envelope waveforms of the low-level offset tone. These curves are plotted with a similar time scale and for four different average input powers.

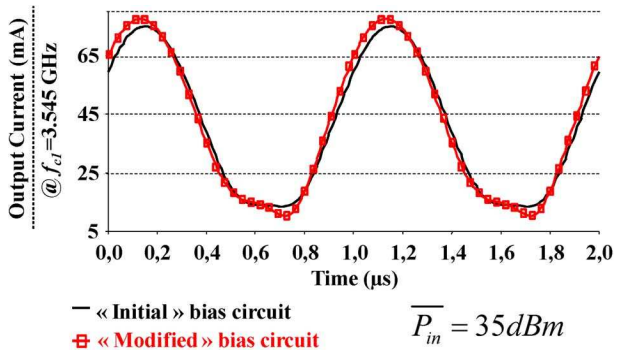

Fig. 22. Comparison of the envelope output current waveforms of the modulated signal at f_{c2} and the low-level tone at f_{c1} for a 35-dBm average input power and for two bias circuit configurations.

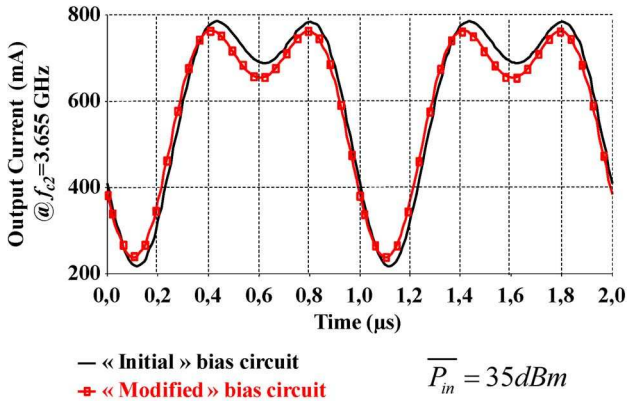

Fig. 23. Comparison of the envelope output current waveforms of the modulated signal at f_{c2} and the low-level tone at f_{c1} for a 35-dBm average input power and for two bias circuit configurations.

These curves are extracted from measurements of time-domain envelope waveforms at the output of the modified power amplifier.

Curves of Figs. 20 and 21 again provide a visual inspection of the transfer modulation phenomenon for a wide frequency offset of 120 MHz.

These results prove the capability of the instrument to measure microwave broadband time-domain waveforms (envelope and carriers components) at both ports of nonlinear devices. The modifications of the envelope output current due to the presence of weak memory effects (initial bias circuit) or more significant memory effects (modified bias circuit) are shown in Figs. 22 and 23 after applying a time alignment process [13].

Although the different shapes of the output current waveforms around f_{c1} measured in the cases of the initial and modified bias circuit configurations do not show the presence of a large amount of memory effects, they prove an interesting capability of the proposed setup.

IV. Conclusion

In this paper, we have presented a broadband calibrated four-channel time-domain measurement system for the characterization of nonlinear devices like power amplifiers. We have proposed a novel hardware architecture of sampling heads and IF circuits to perform broadband time-domain measurements of modulated signals at both ports of the power amplifiers.

Further investigations concern the improvement of the dynamic range of this system, which is limited here to 50 dB. Despite the problem of perfectible signal-to-noise ratio (SNR), this characterization setup has proven to be a valuable tool to aid in characterizing power amplifiers driven by nonadjacent multiple signals. It can be applied to other devices like LNAs. Finally, the measurement tool is also expected to be useful for the behavioral modeling of nonlinear devices with memory [12].

Acknowledgment

The authors wish to acknowledge W. Rebernack, THALES, Colombes, France, for his helpful technical assistance and the Délégation Générale pour l'armement for its technical expertise.

References

[1] M. Sanduleanu, M. Vidojkovic, V. Vidojkovic, A. Van Roermund, and A. Tasic, "Receiver front-end circuits for future generations of wireless communications," *IEEE Trans. Circuits Syst. II, Exp. Briefs*, vol. 55, no. 4, pp. 299–303, Apr. 2008.

[2] M. Brandolini and F. Svelto, "Reconfigurable Si RF receiver front-ends for multi-standard radios," in *Proc. 1st Eur. Wireless Technol. Conf.*, Oct. 2008, pp. 33–36.

[3] C. J. Clark, G. Chrisikos, M. S. Muha, A. A. Moulthrop, and C. P. Silva, "Time-domain envelope measurement technique with application to wideband power amplifier modeling," *IEEE Trans. Microw. Theory Tech.*, vol. 46, no. 12, pp. 2531–2540, Dec. 1998.

[4] F. Macraigne, T. Reveyrand, C. Maziere, D. Barataud, J. M. Nebus, R. Quere, and A. Mallet, "A fully calibrated four channels time domain RF envelope measurement system for the envelope characterization of nonlinear devices in a load-pull environment," in *Eur. Microw. Conf.*, Oct. 4–6, 2005, vol. 2, pp. 729–732.

[5] D. J. Williams, J. Leckey, and P. J. Tasker, "Envelope domain analysis of measured time domain voltage and current waveforms provide for improved understanding of factors effecting linearity," in *IEEE MTT-S Int. Microw. Symp. Dig.*, Jun. 2003, pp. 1411–1414.

[6] M. El Yaagoubi, G. Neveux, D. Barataud, T. Reveyrand, J.-M. Nebus, F. Verbeyst, F. Gizard, and J. Puech, "Time-domain calibrated measurements of wideband multisines using a large-signal network analyzer," *IEEE Trans. Microw. Theory Tech.*, vol. 56, no. 5, pt. 1, pp. 1180–1192, May 2008.

[7] W. Van Moer and Y. Rolain, "An improved broadband conversion scheme for the large signal network analyzer," in *IEEE MTT-S Int. Microw. Symp. Dig.*, Jun. 12–17, 2005, pp. 1501–1504.

[8] M. El Yaagoubi, G. Neveux, D. Barataud, J. M. Nebus, and J. Verspecht, "Accurate phase measurements of broadband multitone signals using a specific configuration of a large signal network analyzer," in *IEEE MTT-S Int. Microw. Symp. Dig.*, Jun. 2006, pp. 1448–1451.

[9] M. Abouchahine, A. Saleh, G. Neveux, T. Reveyrand, J. P. Teyssier, D. Barataud, and J. M. Nebus, "Broadband time domain measurement system applied to the characterization of cross modulation in nonlinear microwave devices," in *IEEE MTT-S Int. Microw. Symp. Dig.*, Boston, MA, Jun. 2009, pp. 1201–1204, Art. ID TH2D-2.

[10] A. Zhu, P. Draxler, C. Hsia, T. Brazil, D. Kimball, and P. Asbeck, "Digital predistortion for envelope-tracking power amplifiers using decomposed piecewise Volterra series," *IEEE Trans. Microw. Theory Tech.*, vol. 56, pp. 2237–2247, Oct. 2008.

[11] L. Bacque, P. Bouysse, W. Rebernak, C. Poumier, L. Lapierre, G. Nanfack-Nkondem, G. Neveux, D. Barataud, and R. Quere, "High current—High speed dynamic bias control system applied to a 100-W wideband push–pull amplifier," *IEEE Trans. Microw. Theory Tech.*, vol. 56, no. 12, pp. 2798–2807, Dec. 2008.

[12] F. Macraigne, T. Reveyrand, G. Neveux, D. Barataud, J. M. Nebus, A. Soury, and E. Ngoya, "Time-domain envelope measurements for characterization and behavioral modeling of nonlinear devices with memory," *IEEE Trans. Microw. Theory Tech.*, vol. 54, no. 8, pp. 3219–3226, Aug. 2006.

[13] G. Nanfack-Nkondem, J. Santiago, G. Neveux, D. Barataud, J. M. Collantes, J. Portilla, C. J. M. Nebus, and A. MAllet, "Characterization of Galileo signal correlation losses caused by non linear power amplification with memory," in *IEEE MTT-S Int. Microw. Symp. Dig.*, Atlanta, GA, Jun. 2008, pp. 1581–1584.

Mouhamad Abouchahine was born in Almanara, Lebanon, on May 12, 1983. He is currently working toward the Ph.D. degree in electronics at the University of Limoges, Limoges, France.

His research interests include the wideband time-domain characterization of RF and microwave nonlinear components.

Alaa Saleh was born in Saida. Lebanon, on August 23, 1983. He is currently working toward the Ph.D. degree in electronics at the University of Limoges, Limoges, France.

His research interests include high-frequency transistor modeling for high-speed digital circuit applications, as well as for microwave samplers.

Guillaume Neveux was born in Civray, France, in 1976. He received the Diplôme d'Etudes Approfondies (DEA) degree from the Université Paris 11, Orsay, France, in 2000, and the Ph.D. degree in electronics and communications from the National Superior Institute of Telecommunications (ENST), Paris, France, in 2003.

Since 2004, he has been with the Instrumentation Group, XLIM Laboratory, University of Limoges, Limoges, France. His research interests include nonlinear measurement with LSNA and the study of RF sampling systems.

Tibault Reveyrand was born in Paris, France, on September 20, 1974. He received the Ph.D. degree from the University of Limoges, Limoges, France, in 2002.

From 2002 to 2004, he was a Post-Doctoral Scientist with the CNES (French Space Agency). In 2005, he became a Contractual CNRS Engineer with XLIM Laboratory (formerly IRCOM), Limoges, France. His research interests include the characterization and modeling of RF and microwave nonlinear components.

Dr. Reveyrand was the recipient of the European GAAS 2002 Best Paper Award.

Jean-Pierre Teyssier was born in Brive, France, in 1963.

Since 1990, he has been with IRCOM/XLIM Laboratory, University of Limoges, Limoges, France. He presented his doctoral thesis in 1994, the subject of which concerned pulsed *I(V)* and pulsed S-parameters for nonlinear characterization of microwave active devices. He has been involved in the design of measurement systems and instrumentation for microwave nonlinear investigations with an emphasis on time-domain pulsed large-signal characterization of transistors. For many years, he and his students have been frequent contributors to ARFTG papers.

Mr. Teyssier is currently a member of ARFTG ExCom, responsible for workshop organization.

Danielle Rousset received the Ph.D. degree from the University of Limoges, Limoges, France, in 1976.

From 1974 to 1981, she was an Assistant Professor with the University of Alger, Alger, Algeria. Since 1982, she has been with the Instrumentation Group, XLIM Laboratory, University of Limoges. Her research interests concern the study of sampling techniques.

Denis Barataud was born in Saint-Junien, France, in 1970. He received the Engineer's degree from the Ecole Nationale Supérieure de Télécommunications de Bretagne, Bretagne, France, in 1994, and the Ph.D. Degree in electronics from the University of Limoges, Limoges, France, in 1998.

From 1998 to 1999, he was a Postdoctoral Scientist with the Microwave Laboratory, CNES, Toulouse, France. Since 2000, he has been with the XLIM (formerly IRCOM) Laboratory, University of Limoges, where in 2001 he became an Assistant Professor. His research interests include the development of time-domain equipment and techniques for the characterization of nonlinear devices.

Jean-Michel Nebus was born in Bourganeuf, France, in 1963. He received the Ph.D. degree in electronics from the University of Limoges, Limoges, France in 1988.

He was a Project Engineer with Alcatel Space Industries, Toulouse, France. He is currently a Professor with the XLIM Laboratory, University of Limoges. His main research interest is nonlinear microwave device characterization and design.